Processing–Structure–Property Relationships in Laser-Annealed PbSe Nanocrystal Thin Films

Benjamin E. Treml,[†] Andrew B. Robbins,[§] Kevin Whitham,[†] Detlef-M. Smilgies,[‡] Michael O. Thompson,[†] and Tobias Hanrath*[,§]

[†]Department of Materials Science and Engineering, [‡]Cornell High Energy Synchrotron Source, and [§]School of Chemical and Biomolecular Engineering, Cornell University, Ithaca, New York 14850, United States

ABSTRACT As nanocrystal (NC) synthesis techniques and device architectures advance, it becomes increasingly apparent that new ways of connecting NCs with each other and their external environment are required to realize their considerable potential. Enhancing inter-NC coupling by thermal annealing has been a long-standing challenge. Conventional thermal annealing approaches are limited by the challenge of annealing the NC at sufficiently high temperatures to remove surface-bound ligands while at the same time limiting the thermal budget to prevent large-scale aggregation. Here we investigate nonequilibrium laser annealing of NC thin films that enables separation of the kinetic and thermodynamic aspects of nanocrystal fusion. We show that laser annealing of NC assemblies on nano- to microsecond time scales can transform initially isolated NCs in a thin film into an interconnected structure in which proximate dots "just touch". We investigate both pulsed laser annealing and laser spike annealing and show that both annealing methods can produce "confined-but-connected" nanocrystal films. We develop a thermal transport model to rationalize the differences in resulting film morphologies. Finally we show that the insights gained from study of nanocrystal mono- and bilayers can be extended to three-dimensional NC films. The basic processing–structure–property relationships established in this work provide guidance to future advances in creating functional thin films in which constituent NCs can purposefully interact.

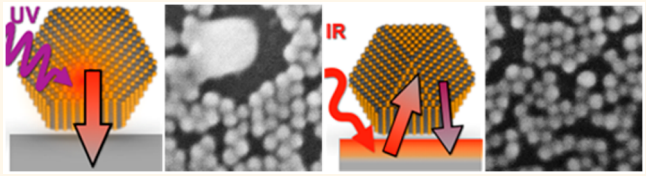

KEYWORDS: nanocrystal · laser annealing · quantum confinement · thin films · diffusion

Advances in the fabrication of materials with nanoscale control over size, shape, and composition have created a fertile opportunity space for novel materials that continues to intrigue scientists and engineers. Semiconductor nanocrystals (NCs), also referred to as quantum dots, in particular provide versatile building blocks for emerging nanotechnologies by virtue of their size-tunable optoelectronic properties and low-cost, solution-based processing.[1−3] To translate this much acclaimed potential to technological fruition, several materials processing and fabrication challenges remain to be resolved; in particular efficiently coupling proximate dots to each other while at the same time preserving the unique quantum-confinement properties of isolated dots persists as a critical challenge. Here we show that the seemingly contradictory requirements can be resolved by rapid nonequilibrium processing techniques.

Previous strategies to improve connections between NCs in thin films can be broadly categorized as chemical and physical approaches. Chemical treatments aim to displace or exchange the native long chain ligand with a shorter ligand. Although these treatments successfully reduce interparticle spacing, chemical treatments generally disrupt long-range ordering of NCs in the film and require layer-by-layer deposition methods.[4−6] Recently, precise control over the chemical treatment of specific NC facets has enabled impressive advances in the formation of superstructures with epitaxial connections among proximate NCs.[7−9] An important concern in chemical treatments is that they introduce significant risks to alter the physical and chemical nature of the NC surface, which, in most cases, has detrimental impacts on the electronic properties. In the specific context of optoelectronic applications of NCs, ligand exchange and displacement have been shown to lead

* Address correspondence to th358@cornell.edu.

Received for review January 9, 2015 and accepted March 18, 2015.

Published online March 18, 2015
10.1021/acsnano.5b00167

to the formation of undesirable surface states that trap mobile charges.[10]

Physical approaches (*e.g.*, thermal annealing or high-pressure treatment) to connect NCs have been less thoroughly explored and present their own challenges. High-pressure processing has been shown to cause oriented fusion of NCs into nanosheets,[11,12] but this approach has not yet been applied to NC thin films in devices. Thermal annealing of NC films provides an ostensibly simple route to reduce interparticle spacing and enhance interdot coupling. However, thermal treatments involve a delicate balance of removing the stabilizing ligands from the NC surface without causing neighboring particles to aggregate. Unfortunately, the relatively high temperatures required to remove surface-bound ligands generally lead to substantial particle aggregation during conventional thermal annealing.[13] *In-situ* TEM studies of NCs with a destabilized ligand shell at elevated temperatures have shown them to rotate and fuse together over time scales as large as minutes *via* surface diffusion.[14]

The degree to which annealed NCs sinter can be described by a diffusion length, $l_d = (D\tau)^{1/2}$. The diffusion coefficient, D, and time, τ, can be tailored by adjusting the temperature and duration of the thermal anneal, respectively. Structural changes of the NC film during thermal annealing can then be qualitatively categorized into three regimes delineated by the ratio of the diffusion length to the nearest neighbor separation between NCs, or l_d/d_{NC}. For $l_d/d_{NC} < 1$, individual NCs effectively stay in their initial position and remain isolated from neighboring particles. On the other hand, for large diffusion lengths, *i.e.*, $l_d/d_{NC} > 1$, particles aggregate into microscopic structures that lack the desired size-tuned properties. At intermediate diffusion lengths, *i.e.*, $l_d/d_{NC} \approx 1$, annealed NCs diffuse and restructure into assemblies in which proximate particles "just touch".

The "confined-but-connected" superstructures, illustrated schematically in Figure 1a, provide the desired balance of quantum confinement (*e.g.*, to tailor light absorption or emission) and interdot coupling (to efficiently transport charges out of and into the NCs). Achieving this delicate processing balance with conventional thermal annealing approaches is complicated since the large temperatures required to remove ligands (200−300 °C) and long annealing times (1−60 min) lead to significant sintering.[15,16]

Restricting the thermal annealing to nano- to microsecond duration provides access to the desired intermediate fusion regime by limiting the extent of particle diffusion. Photonic curing treatment of semiconductor NC films involving pulsed light (160 μs) from a xenon flash lamp was recently demonstrated by Stolle *et al.*[17] The laser annealing approaches explored in this work are illustrated in Figure 1b,c. Pulsed laser annealing (PLA) and laser spike annealing (LSA) provide access to

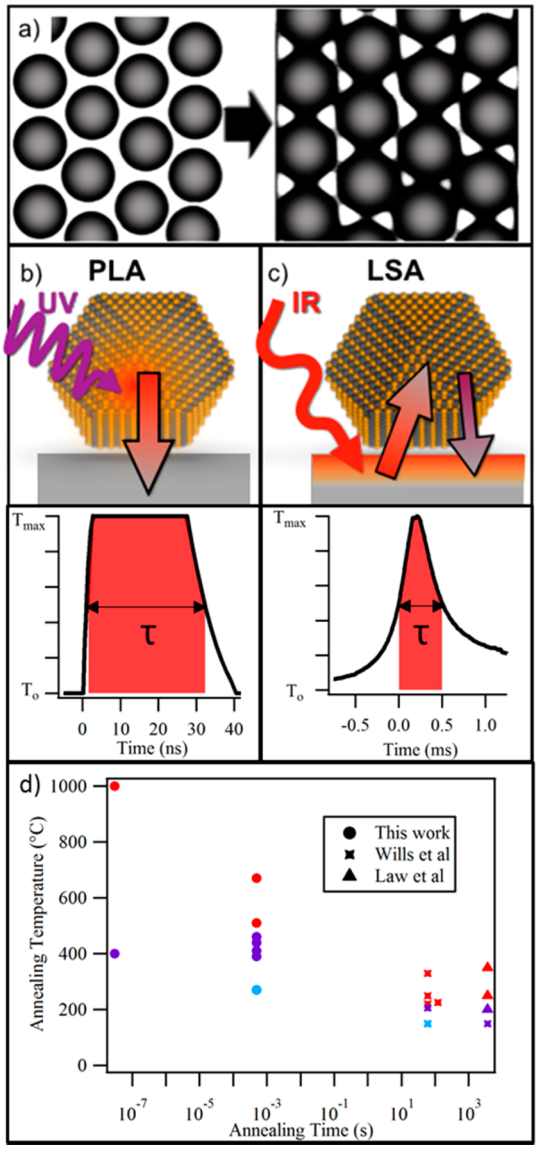

Figure 1. (a) Formation of "confined-but-connected" nanostructures *via* controlled fusion. (b, c) Cartoons of the method of heating for the excimer (b) and CO_2 (c) lasers used in this work. Below, schematic time−temperature profiles for the lasers. Red shading indicates the time during which films are at or above half of the peak temperature. (d) Time−temperature−transformation diagram for annealing of PbSe quantum dots in this and previous works. Red, purple, and blue markers indicate large, intermediate, and small values of l_d, respectively.

different annealing times (ns and μs) and heating strategies (*i.e.*, direct and indirect excitation of the NCs). PLA employs an excimer laser (λ = 308 nm) to deliver a single 30 ns pulse to the entire sample (Figure 1b). The excimer laser pulse is directly absorbed by NCs, resulting in rapid heating followed by rapid thermal quench to the substrate.[18,19] In LSA, on the other hand, a continuous-wave CO_2 laser (λ = 10.6 μm) is scanned across the sample. The infrared laser is absorbed by a highly doped silicon substrate, which conducts heat into the NC film (Figure 1c). Scanning the laser beam across the sample leads to rapid heating

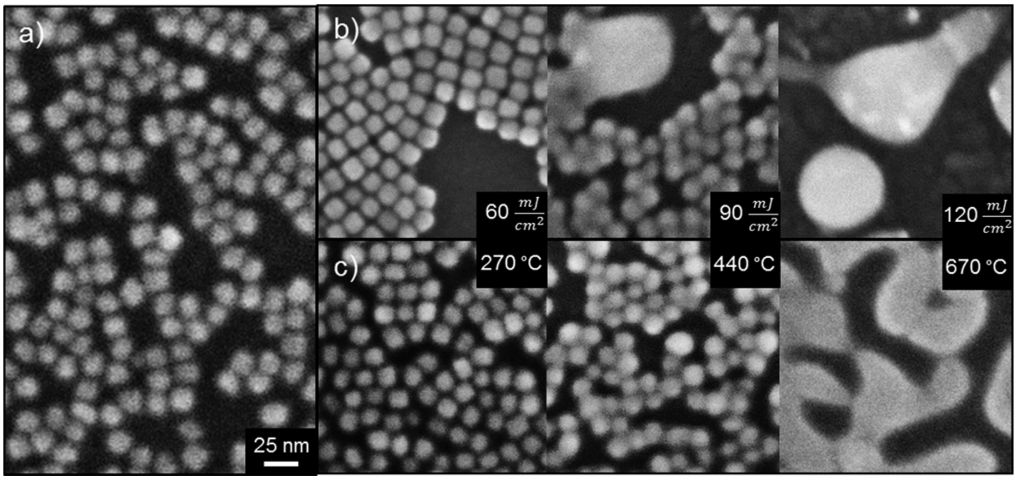

Figure 2. Scanning electron micrographs of (a) an unannealed film and (b, c) PLA and LSA films, respectively. Annealing temperature cannot be determined for PLA films. All micrographs are at the same scale.

as the laser approaches, followed by rapid cooling into the substrate after the laser passes.[20] The duration of the heating can be controlled by the laser scan speed. In the experiments detailed below, we focused on a dwell of 500 μs, defined as the full-width at half-maximum of the laser beam divided by the scan velocity.

Figure 1d compares the characteristic annealing time and temperatures explored in this work to earlier literature reports.[15,16] This plot illustrates that fast thermal processing enabled by laser annealing provides access to substantially higher annealing temperatures than conventional methods. In combination, PLA and LSA present complementary processing techniques to systematically explore a significant region of thermal annealing parameter space.

We focus on PbSe NCs as a model system for the formation of confined-but-connected structures since PbSe NCs provide highly tunable building blocks with well-defined and pronounced quantum confinement effects. Colloidal NCs with precisely controlled size and shape are readily available thanks to robust synthesis methods.[21] The electronic and optical properties of nanostructured PbSe are governed by strong quantum confinement effects.[22] Due to the large Bohr exciton radius of PbSe (23 nm), the optoelectronic properties are highly sensitive to changes in particle size, which provides a clear and strong indicator for change in quantum confinement. The nonequilibrium laser annealing of PbSe NCs described in this work shows that novel "confined-but-connected" structures can be created and that the degree of connection can be tuned *via* precise control over the annealing parameters.

RESULTS AND DISCUSSION

We analyzed the morphology of PbSe NC films with scanning electron microscopy (SEM) before and after laser annealing. For both PLA and LSA laser annealing methods, the NC film morphology can be varied from completely separated NCs to completely sintered structures by controlling the laser power and hence annealing temperature. Figure 2 summarizes the evolution of the morphology of the NC film for a range of annealing conditions. Figure 2a presents the initial film of isolated NCs in a film with submonolayer coverage. We have identified the processing conditions for both PLA (Figure 2b) and LSA (Figure 2c) treated films that correspond to the three processing regimes discussed above. The left image reflects an annealed film with low diffusion length ($l_d/d_{NC} < 1$). The rightmost image in the sequence illustrates completely fused structures formed under conditions of large diffusion lengths ($l_d/d_{NC} \gg 1$). At intermediate conditions, corresponding to a laser fluence of 90 mJ cm^{-2} for PLA and LSA peak temperatures near 440 °C, we observed confined-but-connected structures in which proximate particles "just touch" but maintain their individual particle character. This processing window of opportunity, defined by $l_d/d_{NC} \approx 1$, provides control over the level of connectivity between NCs and creates structures not accessible by conventional processing methods.

Chemical methods for producing physically connected NCs obtain ordered, epitaxially connected structures *via* facet-specific ligand removal that produces anisotropic interactions to guide rotation and assembly.[9,23] In contrast, laser-annealed NC films show reduced order after annealing, indicating that thermal removal of ligands is isotropic or the short annealing times inhibit rotations; as a result, connections between nanocrystals may consist of grain boundaries or amorphous PbSe.

Although both PLA and LSA show a transition region defined by $l_d \approx d_{NC}$, we found that the structures formed by direct PLA were less uniform than NC films annealed indirectly by the LSA method. SEM image analysis of PLA-treated NC films revealed that regions that appear to have melted and completely fused are nanometers away from sections of film that

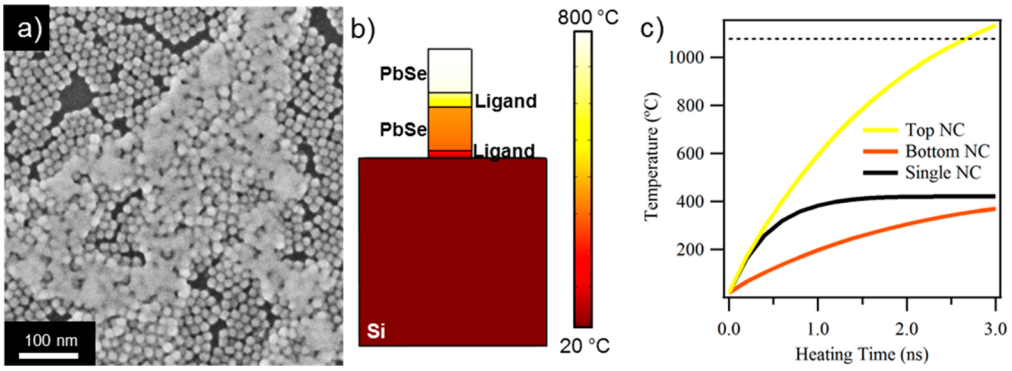

Figure 3. Heat transport under direct absorption of light. (a) Partial bilayer of NCs showing significant sintering in the top layer and limited sintering in a nearby monolayer. (b) Simulated temperature profiles for a bilayer of 12 nm PbSe cubes after 1.6 ns of annealing. (c) Evolution of NC temperature over 3 ns of heating. The dotted line indicates the melting point of PbSe.

are hardly affected by the annealing at all. The variable degree of connection between proximate dots in PLA-treated NC films is undesirable since the structural heterogeneity translates directly into a broad distribution of optical and electrical properties of the NC film.[24,25]

To understand why PLA-treated NC films were less uniform than those treated by LSA, we compared the fundamental heat flows involved in both processes. In the case of LSA, the NCs are not directly photoexcited by the CO_2 laser as the dots are transparent at long wavelengths. Instead, the CO_2 laser is absorbed by the underlying highly doped Si substrate, which then indirectly heats the NC film at the surface. Heat transfer into and out of the NC is therefore by conduction. Following the procedure detailed in recent work by Ong *et al.*, we estimate the thermal conductivity of our NC films to be 0.3 W m^{-1} K^{-1}, which leads to a thermal diffusion length of 800 nm in 1 μs.[26] We can therefore conclude that NCs in monolayer and partial bilayer films are exposed to essentially the same time–temperature profile, leading to a uniform NC film after annealing.

In contrast, the excimer laser employed in PLA is directly absorbed in the NC film. The temperature of the NC therefore depends on the balance of heat generated by thermalization of the direct photoexcitation and heat transferred to the underlying substrate. The effects of direct photoexcitation and limited heat transfer out of the dot are particularly pronounced in partial NC bilayer films. SEM images of partial NC bilayer films annealed with the excimer laser (Figure 3a) reveal that NCs in the top layer are completely fused, whereas the character of individual NCs in the bottom layer is preserved. The dramatically different morphologies formed in the top and bottom layer are a manifestation of the limiting heat transfer out of photoexcited dots. Thicker regions of the film absorb more light and conduct heat away more slowly, which leads to higher temperatures and larger diffusion lengths, l_d.

To better understand the interplay of light absorption and heat transport, we developed an analytical model for the steady state of the system that balances absorbed energy with heat transport into the substrate *via* conduction. Since the thermal conductivity of the Si substrate is approximately 3 orders of magnitude higher than NC films, we can consider the substrate as a room-temperature heat sink. The temperature differential between the NC and the substrate can then be described by $\Delta T = I\rho_{th}$, where I is the absorbed power per unit area and ρ_{th} is the thermal resistance of the NC film. We provide values of the NC absorption coefficients, used to determine the absorbed energy, and thermal conductivities of the NC core and ligand, as well as an example calculation, in the Supporting Information.

In the case of an NC monolayer, the model predicts a steady-state temperature difference of 420 °C at 90 mJ cm^{-2} fluence. In the bilayer case, 50% more energy is absorbed and heat transport must occur across additional thermally resistive NC–ligand interfaces. As a result, the model predicts a temperature differential of 1580 °C, significantly above the melting temperature of PbSe (1083 °C). The basic heat transfer model therefore successfully explains the pronounced differences in pulsed laser annealing of monolayer and bilayer NC films.

Beyond the basic temperature differential, we also sought to understand the transient behavior of the temperature profiles resulting from the short ($\tau \approx$ 30–50 ns) annealing time characteristic for PLA. To simulate the temporal evolution of the temperature in the NC film, we modeled NC monolayer and bilayer films in COMSOL (details of the model are provided in the Supporting Information). Figure 3c compares the simulated temperature transients for monolayer and bilayer NC films during the first 3 ns of heating with a 90 mJ cm^{-2} excimer laser pulse. We can see that the monolayer film reaches the predicted steady-state temperature very quickly. In the case of a bilayer, the top NC rises past the melting point of PbSe after only 3 ns of heating.

The significantly higher temperature of the NC in the top layer is consistent with the NC coalescence revealed in our experiments. Figure 3b shows a snapshot of the model 1.6 ns after the heating pulse. The PbSe NC cores are nearly isothermal, while temperature drops occur in the ligands that separate the NCs. This temperature gradient is consistent with the MD simulations of a 1D chain of NCs by Ong *et al.*[26] Our model indicates that due to increased absorption of energy as well as decreased thermal transport away from heated NCs, the precise thickness of a NC film has a large impact on the temperatures experienced due to direct heating. The large variation in temperature exacerbates inhomogeneities in the NC film, leading to a nonuniform film after processing. Collectively, experiments and the simulation shown in Figure 3 underscore that the morphology of the PLA-treated NCs depends critically on the thickness (*i.e.*, monolayer *vs* bilayer) coverage of the NC film.

Building on the basic processing−structure relationships established for the mono- and bilayer NC films discussed above, we sought to understand how laser annealing transforms the structure of thicker multilayered NC films. In particular, we were interested to study how the structure of an ordered 3D NC superlattice may be transformed during laser annealing. Whereas SEM analysis can provide valuable information about the morphological changes of mono- and bilayer NC films, electron microscopy is generally inadequate to gain detailed insights into the three-dimensional structure of the superlattice. To resolve this challenge, we turned to grazing incidence small-angle X-ray scattering (GISAXS) to probe three-dimensional structural changes in multilayer NC superlattices during laser annealing. The large thermal diffusion length for NC films treated with LSA ensures that thicker (~50 nm) films follow the same time−temperature profiles as the monolayers studied earlier. GISAXS patterns in Figure 4 reveal that NC films are initially ordered in an FCC superlattice structure with (111) superlattice planes parallel to the substrate. Annealing at 440 °C leads to disorder in the film, as evidenced by the loss of diffraction peaks and increased intensity in a ring indicating a loss of orientational order. We attribute the partial loss of film order to the limited fusion among particles, as observed in the SEM studies. Annealing at higher temperatures leads to a complete destruction of NC superlattice order, and only the NC form factor is apparent in GISAXS.

To gain insight into changes of the electronic structure and degree of quantum confinement in the nanostructured films detailed above, we analyzed the excitonic peak in the optical spectrum of PbSe nanostructures. By virtue of the large Bohr exciton radius, the optical properties of PbSe NCs are highly sensitive to particle size; therefore analysis of the evolution of

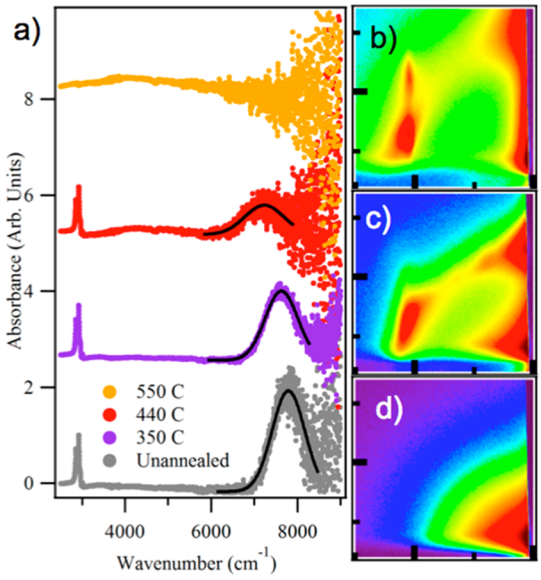

Figure 4. Laser annealing of 3D NC superlattices. (a) FTIR absorption of NC superlattices after annealing. The black line represents a Gaussian fit to the excitonic peak. (b, c, d) GISAXS patterns of samples unannealed and annealed at 440 and 550 °C, respectively. Bold ticks indicate 1 nm^{-1}.

excitonic peak position and width allows us to probe whether quantum-confined electronic structure is preserved or whether large-scale sintering leads to a film with bulk-like optical properties.

Figure 4a illustrates the evolution of the excitonic peak of the initial PbSe NC film compared to LSA-treated NC films for a range of temperatures. The optical spectra show that the excitonic peak was preserved up to annealing temperatures of 440 °C, but lost at higher annealing temperatures, corresponding to aggregated PbSe nanostructures formed under conditions for which $l_d/d_{NN} > 1$. FTIR spectra in Figure 4a also provide insight into the fate of oleic acid ligands bound to the surface of PbSe NC ligands. NC films annealed up to temperatures of 440 °C show characteristic CH stretches near 3000 cm^{-1}, whereas the absence of these vibrational signatures at higher temperatures (550 °C) suggests complete ligand removal. Interestingly, NC films annealed at 440 °C, in the middle of the window of opportunity, reveal an excitonic peak that is red-shifted by 60 meV and broadened, which suggests that this film is less confined than the unannealed film.[27,28] The decrease in confinement is likely due to a combination of an increase in electronic coupling among neighboring particles due to physical connections among particles and an increased effective permittivity, both of which decrease the energy of creating an exciton. Electrical measurements of NC films deposited in the channel of a prefabricated electrode structure show a 300-fold increase in electrical conductivity in response to a 400 °C CO_2 laser annealing treatment (see Figure S2). Taken together, our structural, optical, and electical

characterization of laser-annealed NC films indicates that laser processing can be used to create quantum dot films with tunable morphologies and properties not obtainable *via* conventional processing methods.

CONCLUSION

We investigated pulsed laser annealing and laser spike annealing as nonequilibrium processing methods to create confined-but-connected NC films. Both annealing methods provide a window of opportunity that enables the fabrication of structures with limited physical contact among particles. The comparison of direct (PLA) and indirect (LSA) annealing methods revealed that the latter yields more homogeneous films. We present experimental results and corresponding analytical models to explain the structure transformations in the context of the NC film morphology and heat transfer modes. We showed that insights into processing–structure relationships from the study of mono- and bilayer NC films also guide the laser annealing of thicker three-dimensional NC superlattices. We presented optical spectroscopy of the laser-annealed films to illustrate structure-dependent changes in the extent of quantum confinement of laser-annealed NC films. The basic structure–processing–property relationships established in this work provide valuable guidance to future advances in creating functional thin films in which constituent NCs can purposefully interact *via* nonequilibrium processing.

METHODS

Materials. Lead oxide (99.99%), selenium (99.999%, powder), trioctylphosphine (90%, technical grade), oleic acid (OA 70%, technical grade), 1-octadecene (ODE 90%), and diphenylphosphine (98%) were all purchased from Sigma-Aldrich and used without further purification.

Nanocrystal Synthesis. PbSe NCs were synthesized using a procedure adapted from Yu *et al.*[21] In a typical synthesis 0.88 g of PbO was mixed with 10.8 g of 1-octadecene and 2.76 g of oleic acid in a three-neck flask under nitrogen flow and heated to 150 °C for 1 h until all of the PbO had dissolved. A 90 μL amount of diphenylphosphine was mixed with 12 mL of 1 M selenium in trioctylphosphine and quickly injected into the three-neck flask. Injection temperature and growth time can be adjusted to control the final particle size. The NCs were isolated from the reaction product by washing three times using hexane/ethanol as the solvent/antisolvent pair.

Sample Fabrication. Monolayer and submonolayer samples for SEM characterization were fabricated by drag coating a 10 mg/mL solution of PbSe NCs in hexane across a Si substrate. Thicker films used for GISAXS and FTIR absorption measurements were drop-cast from a 10 mg/mL solution of PbSe NCs in a 9:1 hexane/octane solvent.

Laser Annealing. Excimer annealing was performed using a 308 nm Lambda Physik LPX205i XeCl excimer laser with a 30 ns pulse at full width at half-maximum and a maximum pulse energy of 500 mJ. The beam is homogenized to 3.2 × 3.2 mm^2 square with fluences up to 1.5 J/cm^2. Laser spike annealing was performed by scanning a continuous-wave CO_2 laser (λ = 10.6 μm) across a sample. The laser was focused to a beam with a Gaussian full width half-maximum (FWHM) of 100 μm in the direction of a scan and 500 μm in the lateral direction. Scans were performed at a velocity of 200 mm/s, corresponding to a dwell time of 500 μs. Scans overlapped with a portion of the previous scan to ensure film uniformity.

Characterization. Scanning electron microscopy was performed on a LEO 1550 FESEM. FTIR spectroscopy was performed with a Bruker Hyperion 2000 in ATR mode. GISAXS was performed at the D1 beamline of the Cornell High Energy Synchrotron Source (CHESS) using monochromatic radiation of wavelength 1.161 Å and a bandwidth $\Delta\lambda/\lambda$ = 1.5%. The X-ray beam was produced by a hardbent dipole magnet of the Cornell storage ring and monochromatized with Mo:B_4C synthetic multilayers with a period of 30 Å. GISAXS images were collected by a MedOptics fiber coupled CCD camera with a pixel size of 46.9 μm by 46.9 μm and a total of 1024 by 1024 pixels with 14-bit dynamical range per pixel. The sample to detector distance was 930 mm, as calibrated by a silver behenate powder standard. Images were dark current corrected, distortion corrected, and flat field corrected by the acquisition software. The incident angle of the X-ray beam was 0.25°. Scattering images were calibrated using the Fit2D software.[29]

Conflict of Interest: The authors declare no competing financial interest.

Supporting Information Available: Details of the PLA thermal transport modeling, additional SEM images of confined-but-connected films, electrical conductivity measurements. This material is available free of charge *via* the Internet at http://pubs.acs.org.

Acknowledgment. This work made use of the Cornell Center for Materials Research Shared Facilities, which are supported through the NSF MRSEC program (DMR-1120296). A.B.R. acknowledges support from the Engineering Learning Initiative, College of Engineering, Cornell University. Part of this work is based upon research conducted at the Cornell High Energy Synchrotron Source (CHESS), which is supported by the National Science Foundation and the National Institutes of Health/National Institute of General Medical Sciences under NSF awards DMR-0936384 and DMR-1332208. We would like to thank Alan Jacobs for help with the laser annealing.

REFERENCES AND NOTES

1. Pietryga, J. M.; Schaller, R. D.; Werder, D.; Stewart, M. H.; Klimov, V. I.; Hollingsworth, J. A. Pushing the Band Gap Envelope: Mid-Infrared Emitting Colloidal PbSe Quantum Dots. *J. Am. Chem. Soc.* **2004**, *126*, 11752–11753.
2. Nozik, A. J.; Beard, M. C.; Luther, J. M.; Law, M.; Ellingson, R. J.; Johnson, J. C. Semiconductor Quantum Dots and Quantum Dot Arrays and Applications of Multiple Exciton Generation to Third-Generation Photovoltaic Solar Cells. *Chem. Rev.* **2010**, *110*, 6873–6890.
3. Vineis, C. J.; Beverly, M.; Shakouri, A.; Cruz, S. C.; Majumdar, A.; Kanatzidis, M. G. Nanostructured Thermoelectrics: Big Efficiency Gains from Small Features. *Adv. Mater.* **2010**, *22*, 3970–3980.
4. Talapin, D. V.; Murray, C. B. PbSe Nanocrystal Solids for n- and p-Channel Thin Film Field-Effect Transistors. *Science* **2005**, *310*, 86–89.
5. Liu, Y.; Gibbs, M.; Puthussery, J.; Gaik, S.; Ihly, R.; Hillhouse, H. W.; Law, M. Dependence of Carrier Mobility on Nanocrystal Size and Ligand Length in PbSe Nanocrystal Solids. *Nano Lett.* **2010**, *10*, 1960–1969.
6. Luther, J. M.; Law, M.; Song, Q.; Perkins, C. L.; Beard, M. C.; Nozik, A. J. Structural, Optical, and Electrical Properties of Self-Assembled Films of PbSe Nanocrystals Treated with 1,2-Ethanedithiol. *ACS Nano* **2008**, *2*, 271–280.
7. Schliehe, C.; Juarez, B. H.; Pelletier, M.; Jander, S.; Greshnykh, D.; Nagel, M.; Meyer, A.; Foerster, S.; Kornowski, A.; Klinke, C.

Ultrathin PbS Sheets by Two-Dimensional Oriented Attachment. *Science* **2010**, *329*, 550–553.
8. Boneschanscher, M. P.; Evers, W. H.; Geuchies, J. J.; Altantzis, T.; Goris, B.; Rabouw, F. T.; van Rossum, S. A. P.; van der Zant, H. S. J.; Siebbeles, L. D. A.; Van Tendeloo, G.; Swart, I.; Hilhorst, J.; Petukhov, A. V.; Bals, S.; Vanmaekelbergh, D. Long-Range Orientation and Atomic Attachment of Nanocrystals in 2D Honeycomb Superlattices. *Science* **2014**, *344*, 1377–1380.
9. Baumgardner, W. J.; Whitham, K.; Hanrath, T. Confined-but-Connected Quantum Solids *via* Controlled Ligand Displacement. *Nano Lett.* **2013**, *13*, 3225–3231.
10. Katsiev, K.; Ip, A. H.; Fischer, A.; Tanabe, I.; Zhang, X.; Kirmani, A. R.; Voznyy, O.; Rollny, L. R.; Chou, K. W.; Thon, S. M.; *et al*. The Complete in-Gap Electronic Structure of Colloidal Quantum Dot Solids and Its Correlation with Electronic Transport and Photovoltaic Performance. *Adv. Mater.* **2014**, *26*, 937–942.
11. Wang, Z.; Schliehe, C.; Wang, T.; Nagaoka, Y.; Cao, Y. C.; Bassett, W. A.; Wu, H.; Fan, H.; Weller, H. Deviatoric Stress Driven Formation of Large Single-Crystal PbS Nanosheet from Nanoparticles and *in Situ* Monitoring of Oriented Attachment. *J. Am. Chem. Soc.* **2011**, *133*, 14484–14487.
12. Li, W.; Fan, H.; Li, J. Deviatoric Stress-Driven Fusion of Nanoparticle Superlattices. *Nano Lett.* **2014**, *14*, 4951–4958.
13. Goodfellow, B. W.; Rasch, M. R.; Hessel, C. M.; Patel, R. N.; Smilgies, D.-M.; Korgel, B. A. Ordered Structure Rearrangements in Heated Gold Nanocrystal Superlattices. *Nano Lett.* **2013**, *13*, 5710–5714.
14. van Huis, M. A.; Kunneman, L. T.; Overgaag, K.; Xu, Q.; Pandraud, G.; Zandbergen, H. W.; Vanmaekelbergh, D. l. Low-Temperature Nanocrystal Unification through Rotations and Relaxations Probed by *in Situ* Transmission Electron Microscopy. *Nano Lett.* **2008**, *8*, 3959–3963.
15. Law, M.; Luther, J.; Song, Q.; Hughes, B.; Perkins, C.; Nozik, A. Structural, Optical, and Electrical Properties of PbSe Nanocrystal Solids Treated Thermally or with Simple Amines. *J. Am. Chem. Soc.* **2008**, *130*, 5974–5985.
16. Wills, A. W.; Kang, M. S.; Khare, A.; Gladfelter, W. L.; Norris, D. J. Thermally Degradable Ligands for Nanocrystals. *ACS Nano* **2010**, *4*, 4523–4530.
17. Stolle, C. J.; Harvey, T. B.; Pernik, D. R.; Hibbert, J. I.; Du, J.; Rhee, D. J.; Akhavan, V. A.; Schaller, R. D.; Korgel, B. A. Multiexciton Solar Cells of $CuInSe_2$ Nanocrystals. *J. Phys. Chem. Lett.* **2013**, *5*, 304–309.
18. Baumgardner, W. J.; Choi, J. J.; Bian, K.; Fitting Kourkoutis, L.; Smilgies, D.-M.; Thompson, M. O.; Hanrath, T. Pulsed Laser Annealing of Thin Films of Self-Assembled Nanocrystals. *ACS Nano* **2011**, *5*, 7010–7019.
19. Arora, H.; Du, P.; Tan, K. W.; Hyun, J. K.; Grazul, J.; Xin, H. L.; Muller, D. A.; Thompson, M. O.; Wiesner, U. Block Copolymer Self-Assembly-Directed Single-Crystal Homo- and Heteroepitaxial Nanostructures. *Science* **2010**, *330*, 214–219.
20. Iyengar, K.; Jung, B.; Willemann, M.; Clancy, P.; Thompson, M. O. Experimental Determination of Thermal Profiles during Laser Spike Annealing with Quantitative Comparison to 3-Dimensional Simulations. *Appl. Phys. Lett.* **2012**, *100*, 211915.
21. Yu, W. W.; Falkner, J. C.; Shih, B. S.; Colvin, V. L. Preparation and Characterization of Monodisperse PbSe Semiconductor Nanocrystals in a Noncoordinating Solvent. *Chem. Mater.* **2004**, *16*, 3318–3322.
22. Wise, F. W. Lead Salt Quantum Dots: The Limit of Strong Quantum Confinement. *Acc. Chem. Res.* **2000**, *33*, 773–780.
23. Evers, W. H.; Goris, B.; Bals, S.; Casavola, M.; de Graaf, J.; Roij, R. v.; Dijkstra, M.; Vanmaekelbergh, D. Low-Dimensional Semiconductor Superlattices Formed by Geometric Control over Nanocrystal Attachment. *Nano Lett.* **2012**, *13*, 2317–2323.
24. Chandler, R.; Houtepen, A.; Nelson, J.; Vanmaekelbergh, D. Electron Transport in Quantum Dot Solids: Monte Carlo Simulations of the Effects of Shell Filling, Coulomb Repulsions, and Site Disorder. *Phys. Rev. B* **2007**, *75*, 085325.
25. Carbone, I.; Carter, S. A.; Zimanyi, G. T. Monte Carlo Modeling of Transport in PbSe Nanocrystal Films. *J. Appl. Phys.* **2013**, *114*, 193709.
26. Ong, W.; Rupich, S. M.; Talapin, D. V.; McGaughey, A. J.; Malen, J. A. Surface Chemistry Mediates Thermal Transport in Three-Dimensional Nanocrystal Arrays. *Nat. Mater.* **2013**, *12*, 410–415.
27. Moreels, I.; Lambert, K.; De Muynck, D.; Vanhaecke, F.; Poelman, D.; Martins, J. C.; Allan, G.; Hens, Z. Composition and Size-Dependent Extinction Coefficient of Colloidal PbSe Quantum Dots. *Chem. Mater.* **2007**, *19*, 6101–6106.
28. Guyot-Sionnest, P. Electrical Transport in Colloidal Quantum Dot Films. *J. Phys. Chem. Lett.* **2012**, *3*, 1169–1175.
29. Hammersley, A. *FIT2D: an Introduction and Overview*; European Synchrotron Radiation Facility Internal Report ESRF97HA02T; **1997**.